

A Global Drought and Flood Catalogue from 1950 to 2016

Xiaogang He, Ming Pan, Zhongwang Wei, Eric F. Wood, and Justin Sheffield

<https://doi.org/10.1175/BAMS-D-18-0269.2>

Corresponding author: Xiaogang He, hexg@princeton.edu

This document is a supplement to <https://doi.org/10.1175/BAMS-D-18-0269.1> In final form 23 December 2019

©2020 American Meteorological Society

For information regarding reuse of this content and general copyright information, consult the [AMS Copyright Policy](#).



This article is licensed under a [Creative Commons Attribution 4.0 license](#).

Contents

- 1) Inundation and discharge—The fluvial risk
- 2) Table S1
- 3) Figures S1–S17

Inundation and discharge—The fluvial risk

In addition to the traditional flood risk analysis mostly based on streamflow, we use the Catchment-Based Macro-Scale Floodplain model (CaMa-Flood) to simulate floodplain dynamics at the global scale with a particular focus on flood inundation extent (see details in appendix A, “Enhanced routing model” section). We perform fluvial risk analysis to estimate inundation fraction and flood magnitude at different recurrence intervals (i.e., return period) based on fitted generalized extreme value (GEV) distributions globally for the annual maximum flooded area (Fig. S16) and daily streamflow (Fig. S17). Areas of high fractional coverage and flood peaks can be clearly detected from these fluvial (inundation and streamflow) risk maps, including the lower Mississippi River and the western United States, the Amazon and Parana catchments in South America, the Lake Chad, Congo and upper Niger River catchments in Africa, the Indus and Ganges–Brahmaputra–Meghna catchments on the Indian subcontinent, the Yellow, Yangtze, and Songhua River basins in China, the Chao Phraya and Mekong River in Southeast Asia, the Murray Darling, Lake Eyre basin, and Carpentaria Coast in Australia, and the Euphrates and Tigris River catchment in western Asia. As expected, the fraction of flooded area and the flood magnitude both increase with heightened return period. This is especially the case in Amazon, Indus, and Ganges–Brahmaputra–Meghna catchments, where more than 50% of the total 25 km × 25 km grid cell can be flooded. The spatial pattern of these inundation hazard maps (Fig. S16) is consistent with previous modeling studies, although these are based on shorter time periods (e.g., Pappenberger et al. 2012). Similar spatial patterns can be found in the estimated return levels for streamflow (Fig. S17), compared to recently developed operational flooding warning systems [e.g., Global Flood Awareness System (GloFAS); Alfieri et al. 2019]. These inundation hazard maps can be combined with demographic and economic data to study other components of flood risk, such as vulnerability and exposure for impact assessment (Winsemius et al. 2013), similar to the Dartmouth Flood Observatory (DFO), and explicitly include impact indicators, such as people affected and damage estimates.

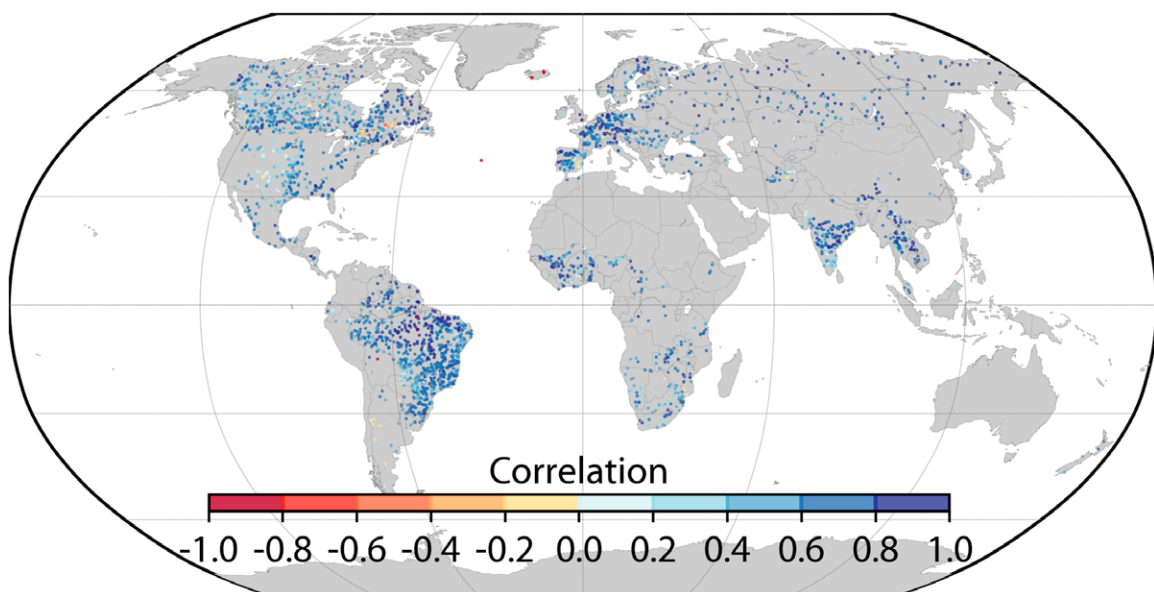


FIG. S1. Monthly streamflow validation results based on correlation coefficient. Only gauges with a drainage area larger than 5,000 km² are selected. Streamflow observations are obtained from the Global Streamflow Indices and Meta data archive (GSIM; Do et al. 2018; Gudmundsson et al. 2018).

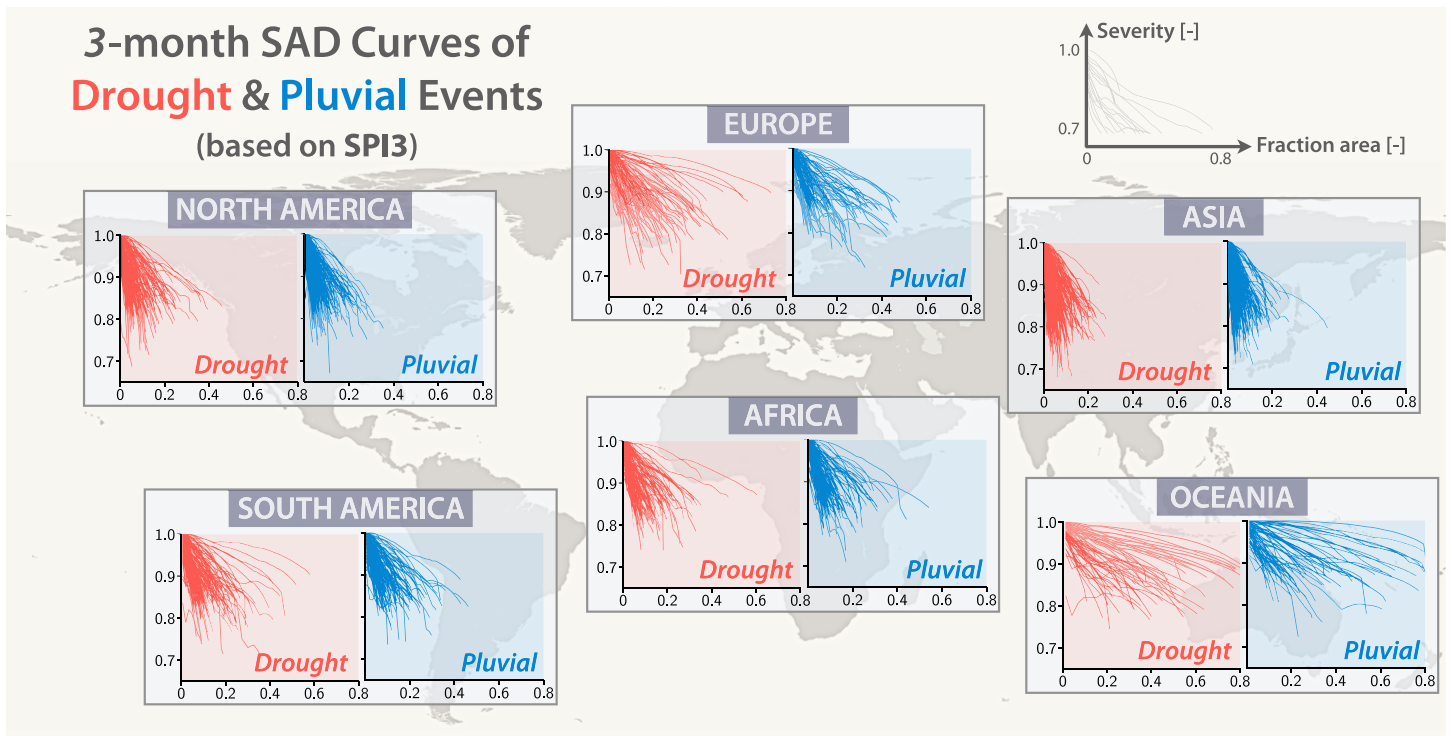


FIG. S2. As in Fig. 3, but drought and pluvial events are detected using SPI3.

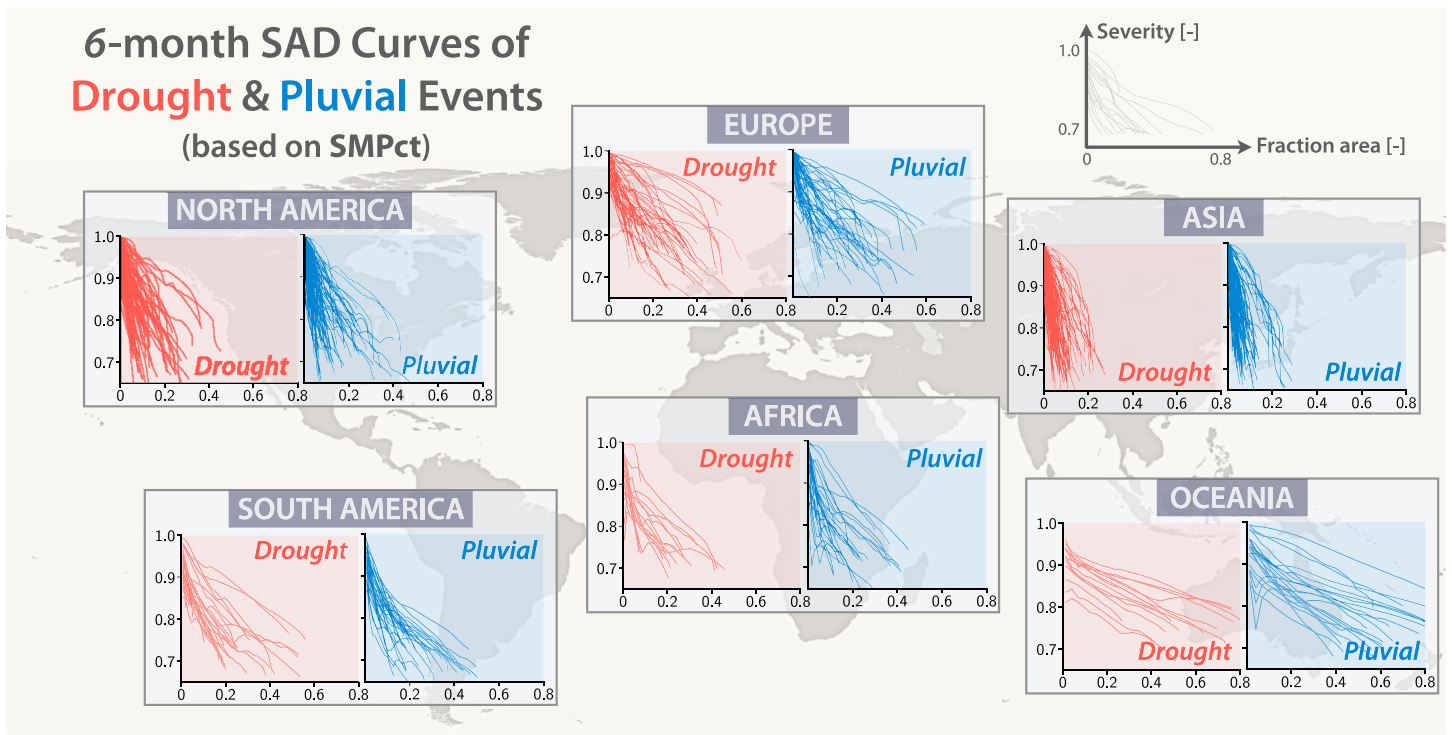


FIG. S3. As in Fig. 3, but for 6-month drought and pluvial events.

6-month SAD Curves of Drought & Pluvial Events (based on SPI3)

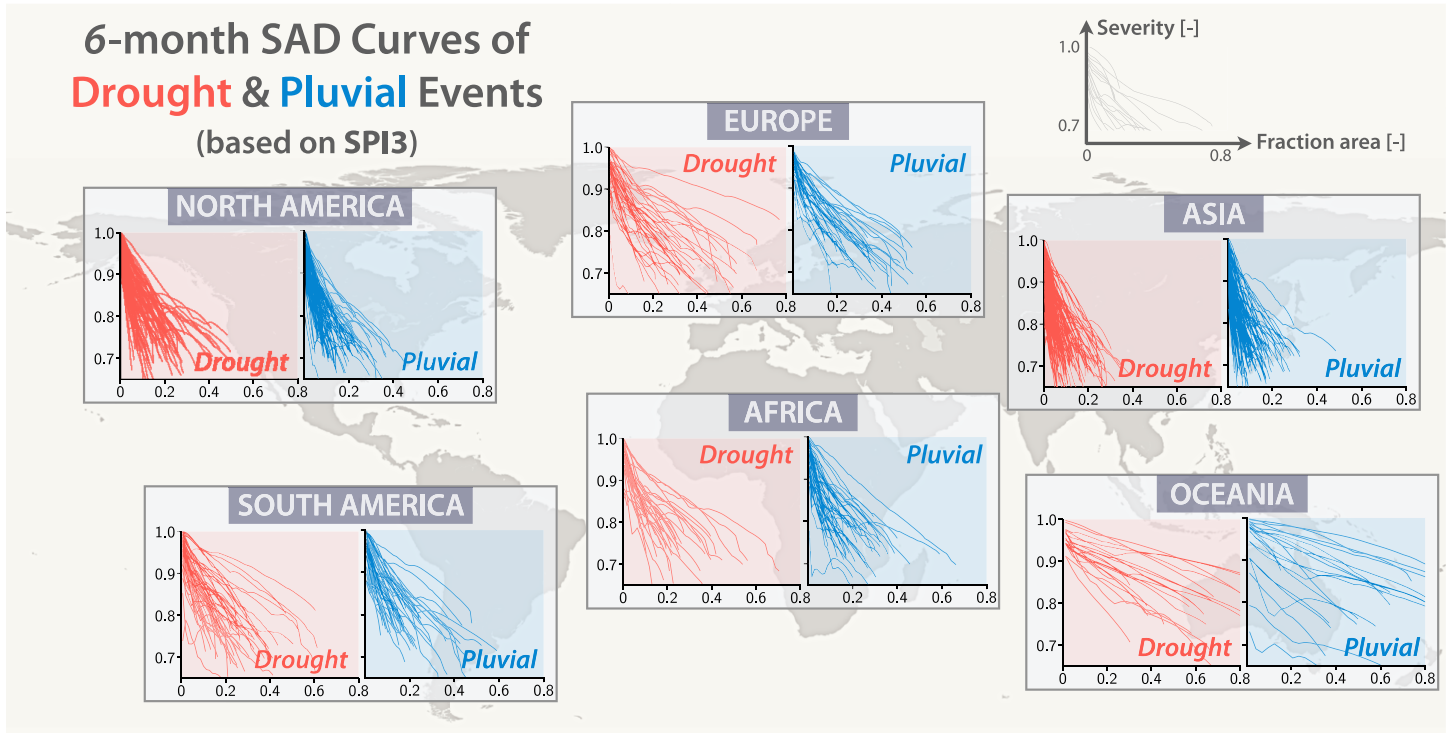


FIG. S4. As in Fig. S3, but drought and pluvial events are detected using SPI3.

9-month SAD Curves of Drought & Pluvial Events (based on SMPct)

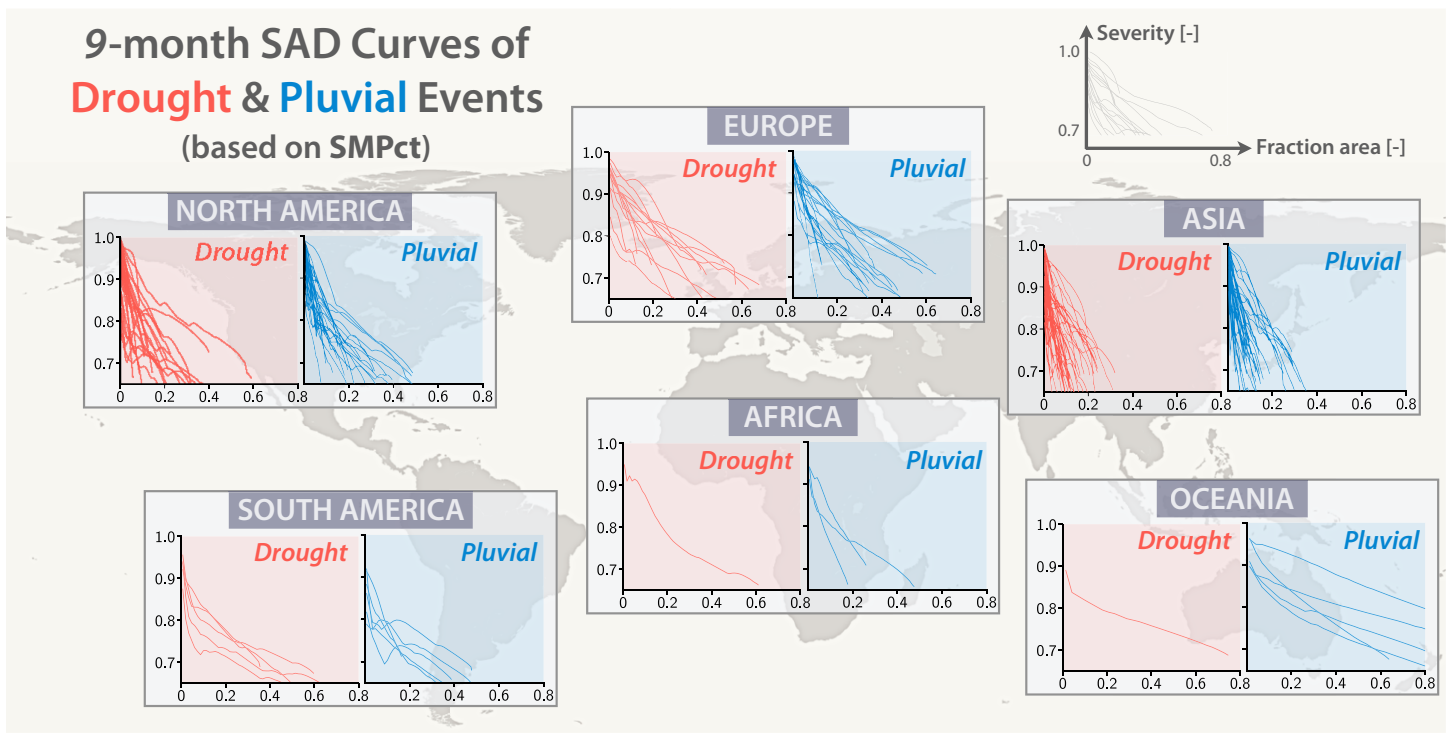


FIG. S5. As in Fig. 3, but for 9-month drought and pluvial events.

9-month SAD Curves of Drought & Pluvial Events (based on SPI3)

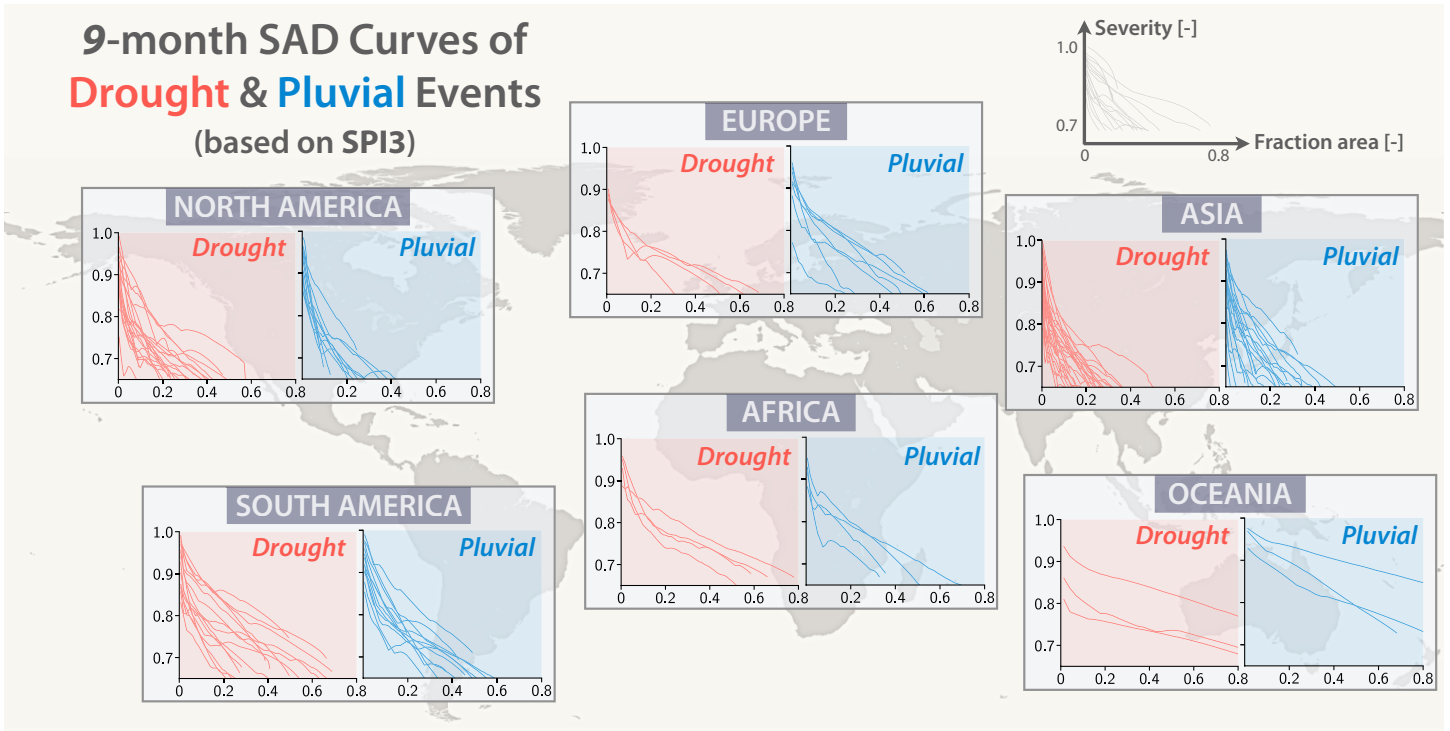


FIG. S6. As in Fig. S5, but drought and pluvial events are detected using SPI3.

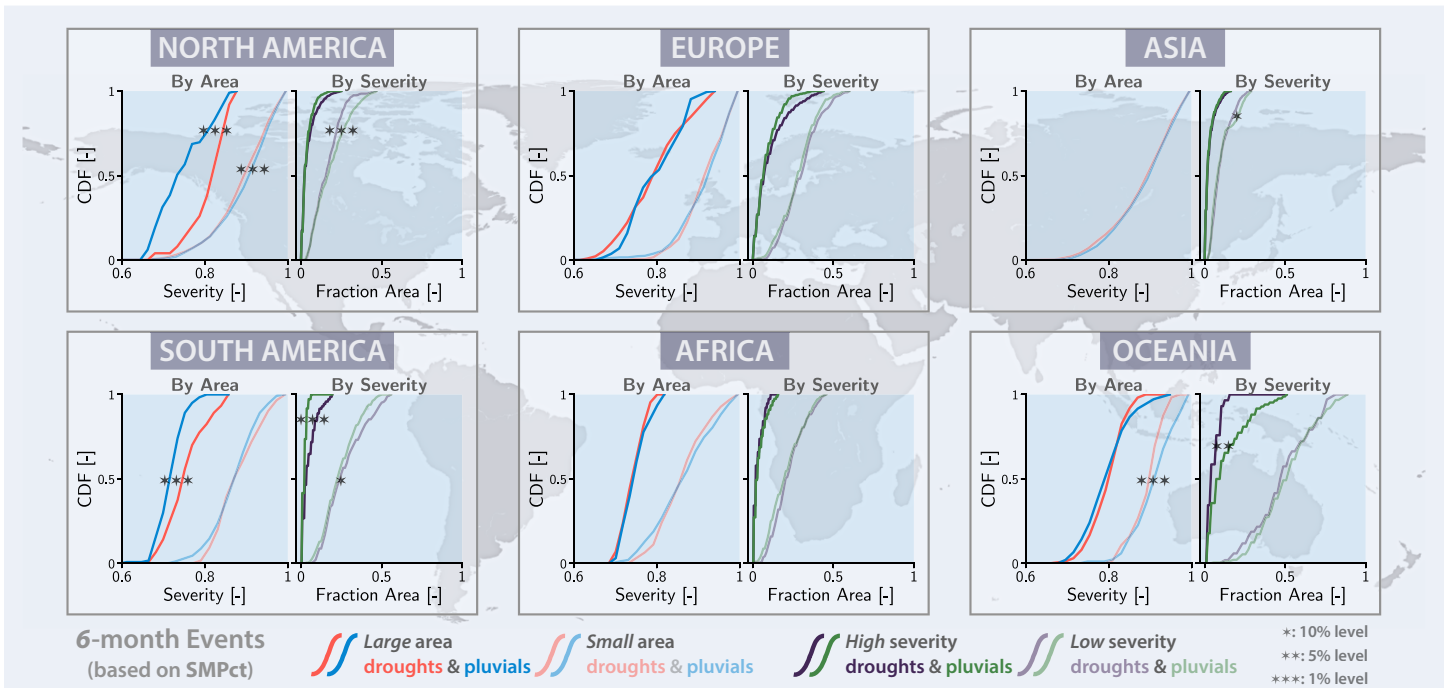


FIG. S7. As in Fig. 4, but for 6-month events.

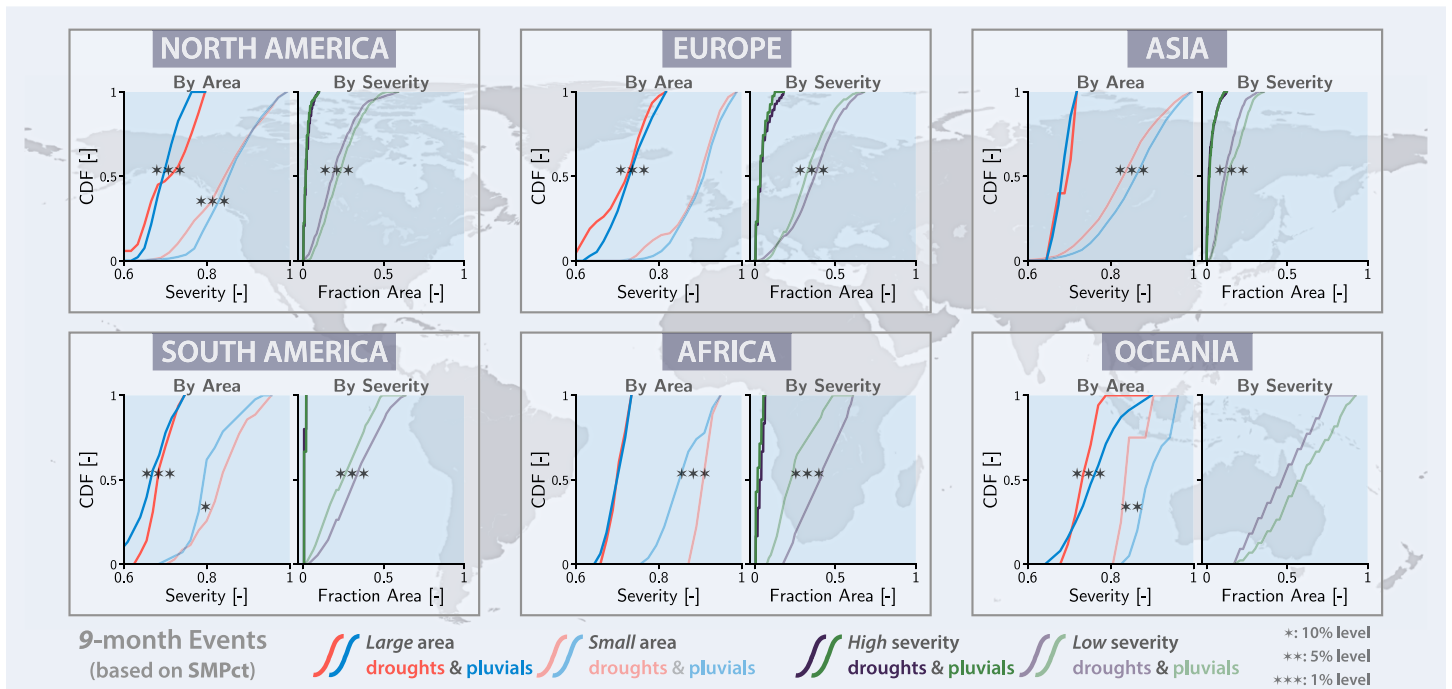


FIG. S8. As in Fig. 4, but for 9-month events.

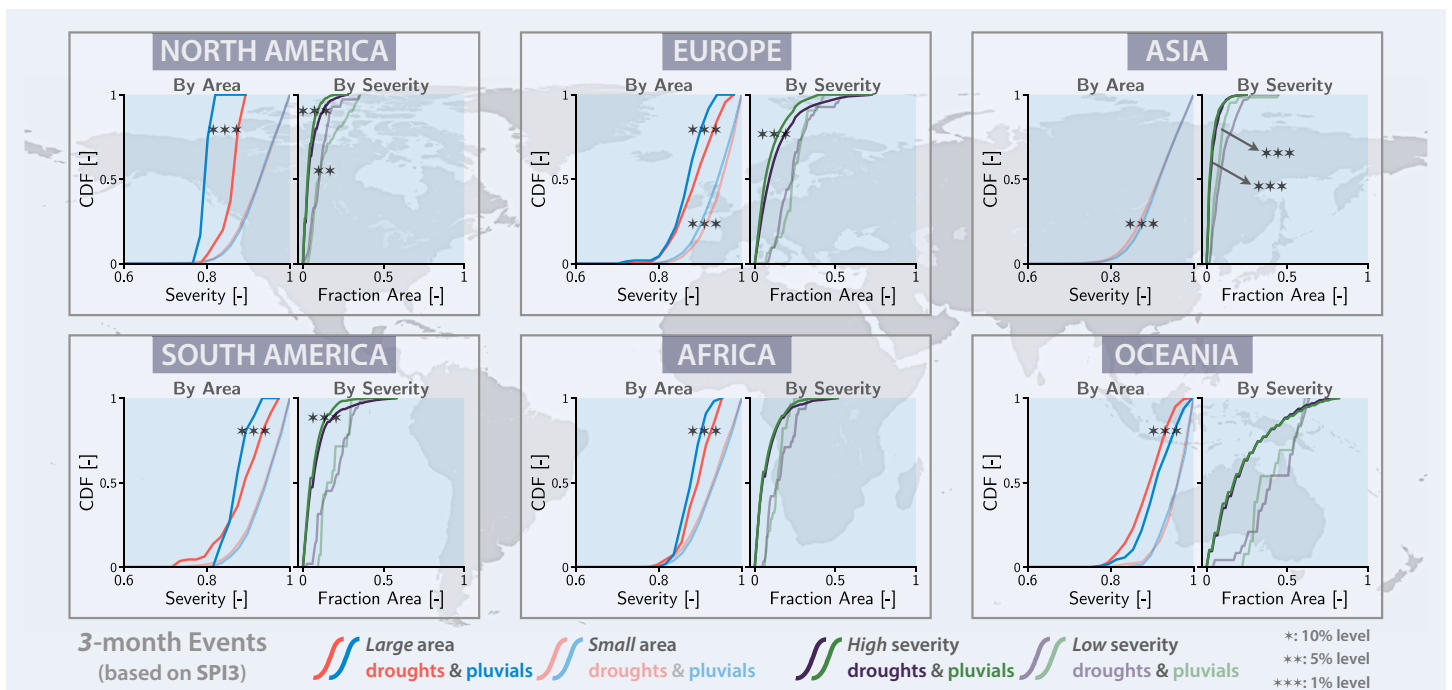


FIG. S9. As in Fig. 4, but drought and pluvial events are detected using SPI3.

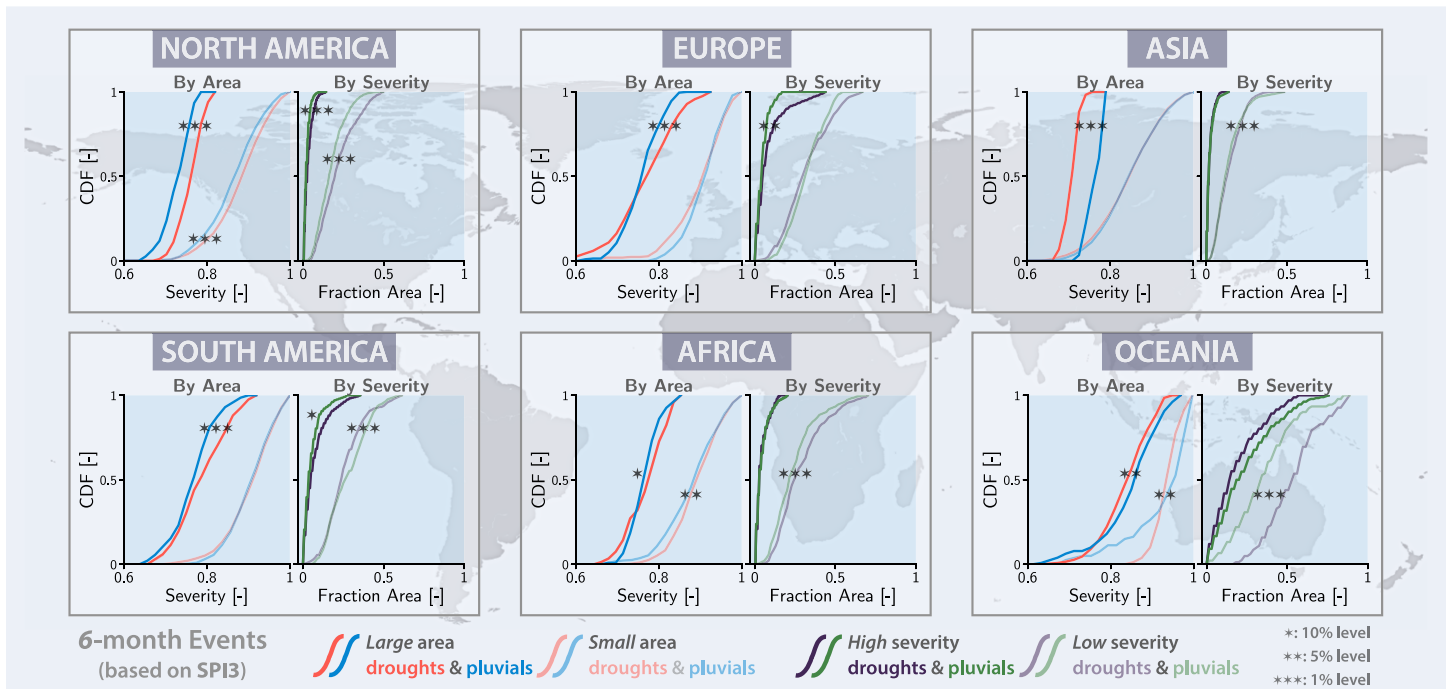


FIG. S10. As in Fig. S9, but for 6-month events.

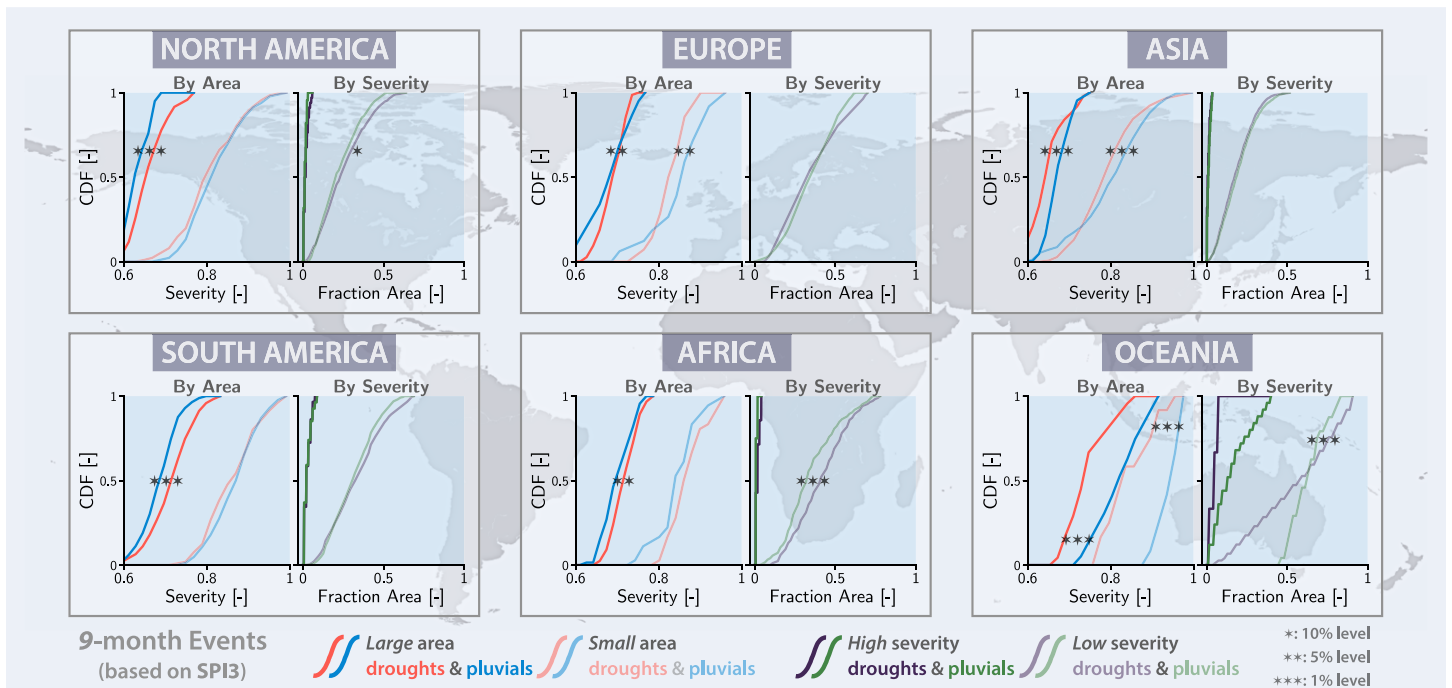


FIG. S11. As in Fig. S9, but for 9-month events.

SAD Envelope Curves of Drought Events

(based on SPI3)

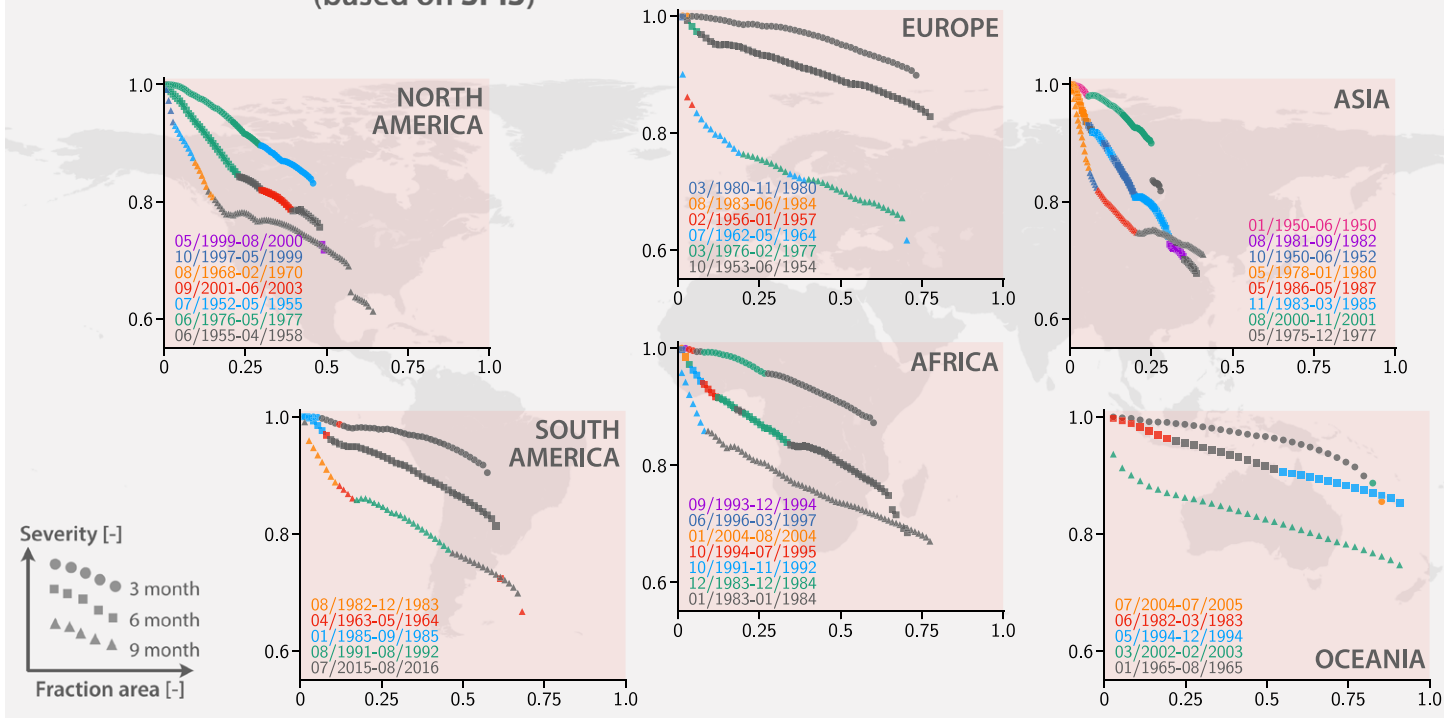


FIG. S12. As in Fig. 7, but drought events are detected using SPI3.

SAD Envelope Curves of Pluvial Events

(based on SPI3)

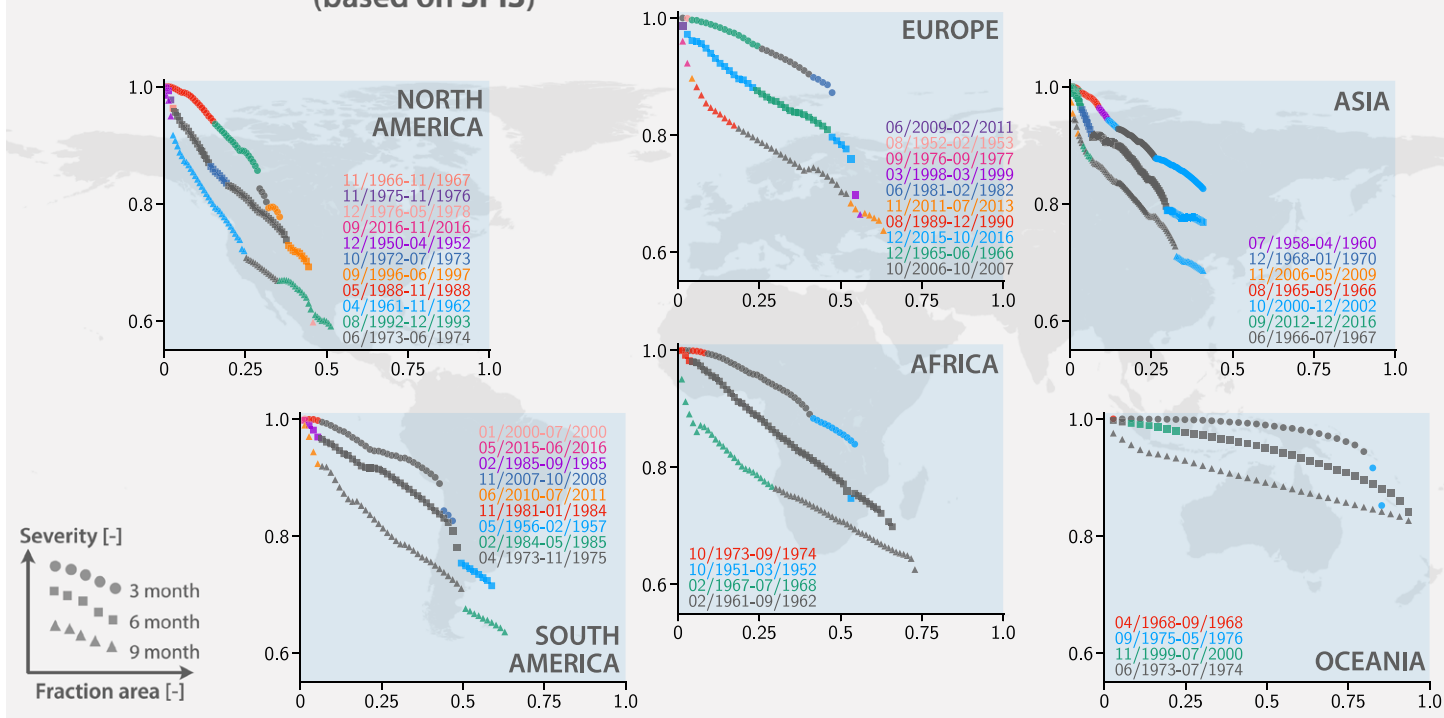


FIG. S13. As in Fig. S12, but for pluvial events.

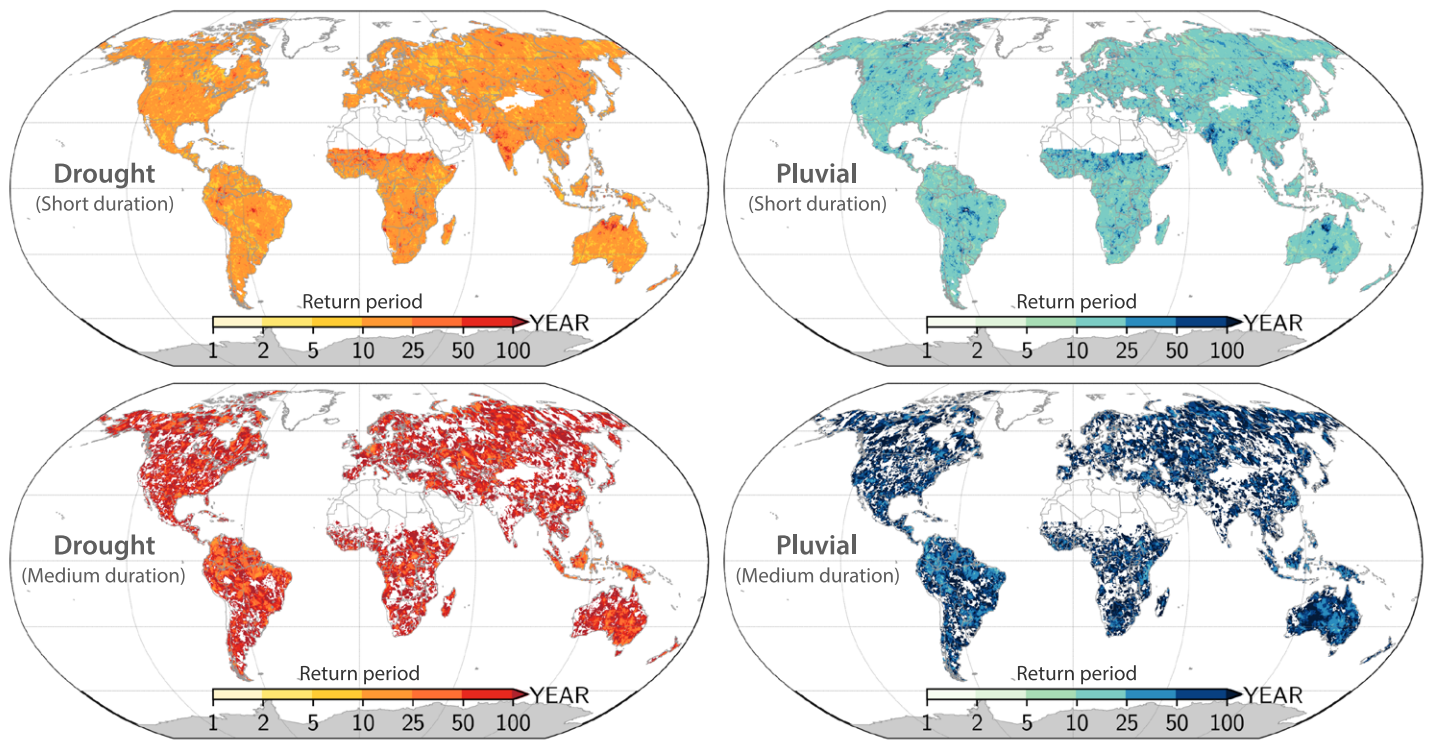


FIG. S14. As in Fig. 9, but droughts and pluvials are identified based on SPI3.

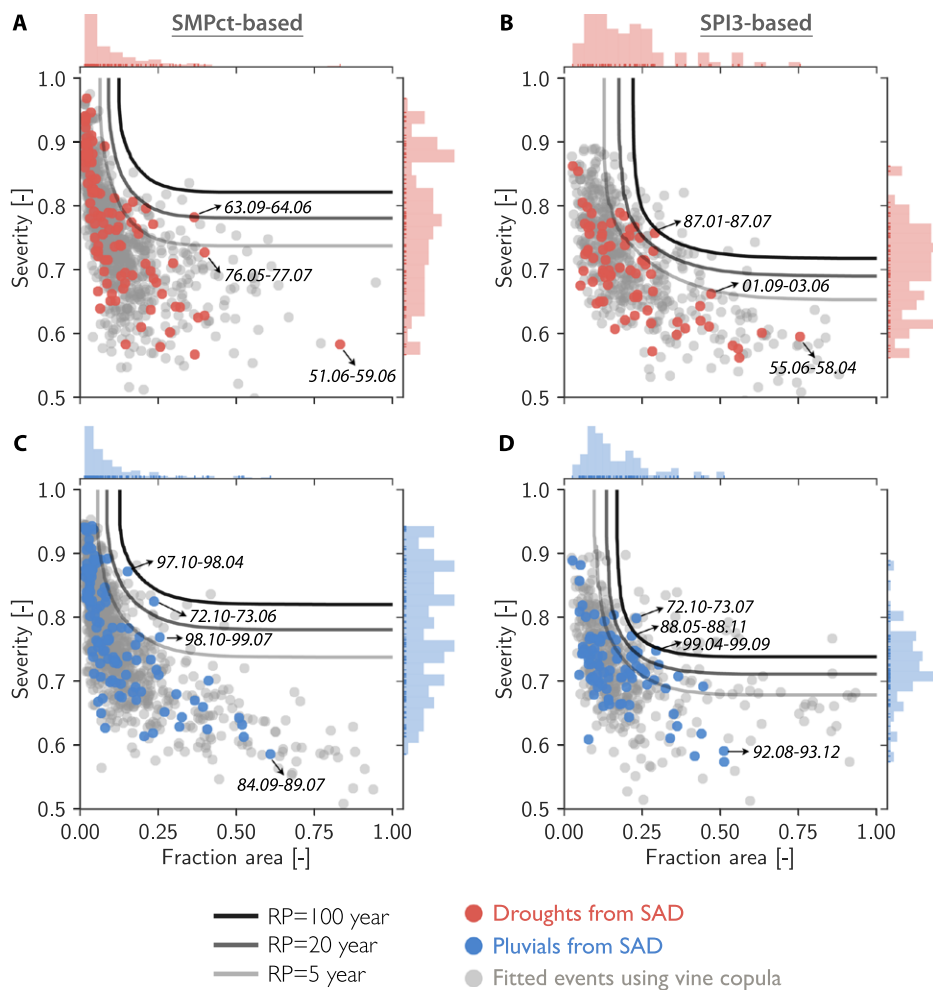


FIG. S15. As in Fig. 10, but for North America.

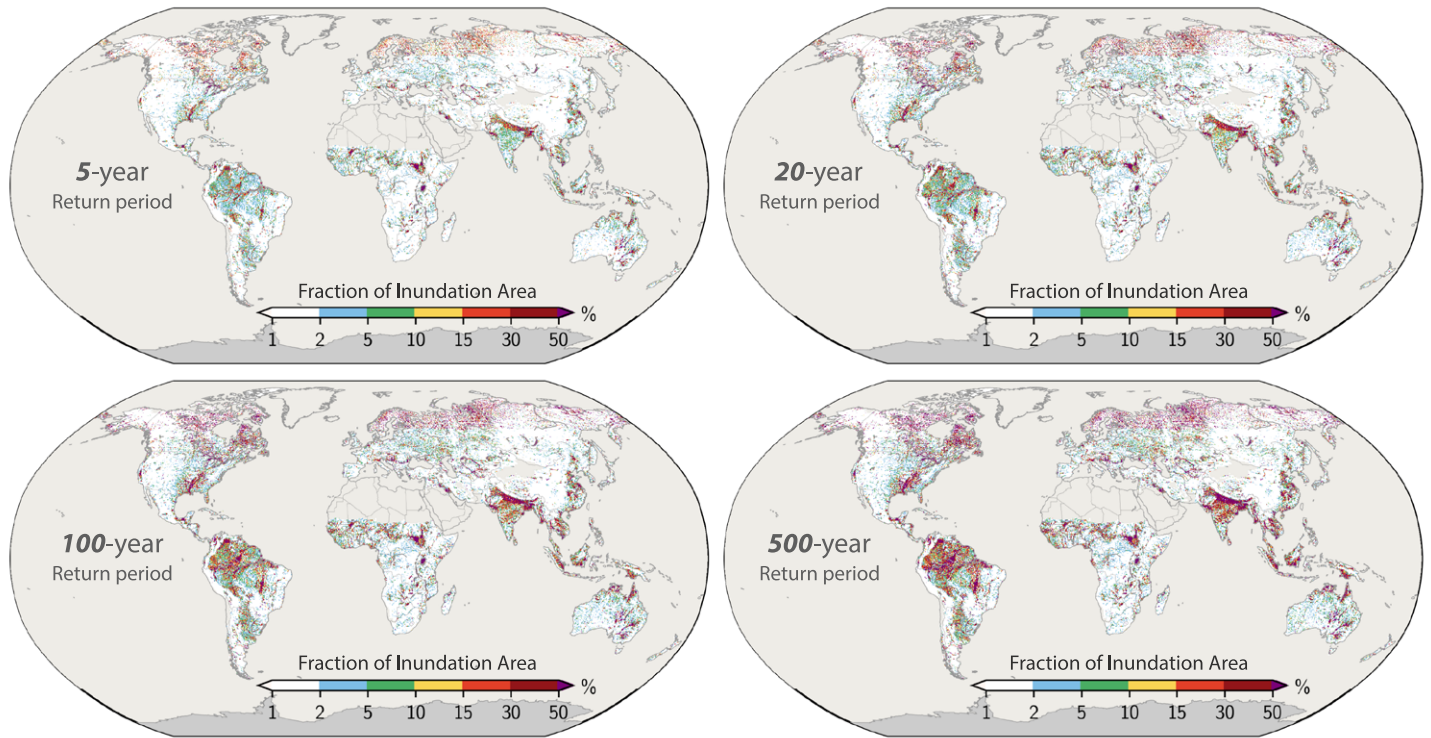


FIG. S16. Annual maximum fractional flooded area for different return periods.

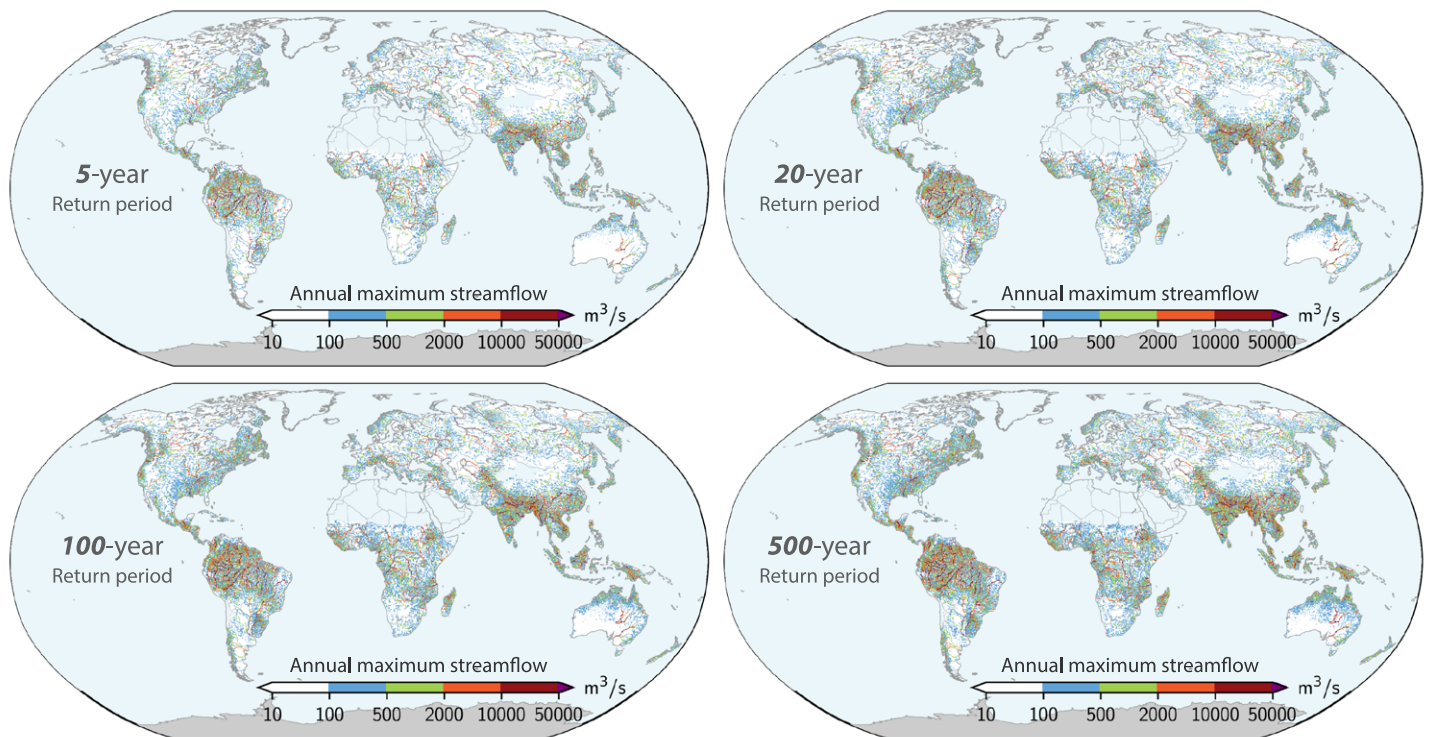


FIG. S17. As in Fig. S16, but for annual maximum daily streamflow.

TABLE S1. List of top five drought and pluvial episodes ranked by duration and spatial extent using both SPI-based and SMPct-based event indices. The duration (months) and fraction area (percentage) under drought or pluvial are given in parentheses. The format for the period of each episode is YYYY.MM–YYYY.MM; for example, 1993.09–1994.12 indicates September 1993–December 1994.

Region	Duration (months)				Spatial extent (fraction %)			
	SPI based		SMPct based		SPI based		SMPct based	
	Drought	Pluvial	Drought	Pluvial	Drought	Pluvial	Drought	Pluvial
Africa	1993.09– 1994.12 (16)	1961.02– 1962.09 (20)	1984.01– 1985.06 (18)	1967.01– 1968.08 (20)	1983.01– 1984.01 (77.9)	1961.02– 1962.09 (73.0)	1984.01– 1985.06 (60.9)	1967.01– 1968.08 (47.5)
	1991.10– 1992.11 (14)	1967.02– 1968.07 (18)	1991.09– 1992.07 (11)	1952.09– 1953.09 (13)	1983.12– 1984.12 (65.9)	1951.10– 1952.03 (58.8)	1982.12– 1983.05 (45.6)	1961.09– 1962.06 (44.8)
	1983.12– 1984.12 (13)	1954.03– 1955.02 (12)	1987.07– 1988.05 (11)	1956.08– 1957.07 (12)	1991.10– 1992.11 (58.5)	1967.02– 1968.07 (52.0)	1991.09– 1992.07 (41.3)	1961.01– 1961.08 (40.7)
	1983.01– 1984.01 (13)	1973.10– 1974.09 (12)	1996.08– 1997.05 (10)	1968.02– 1968.12 (11)	1993.09– 1994.12 (52.9)	1968.12– 1969.06 (39.9)	1983.08– 1984.05 (33.1)	1968.12– 1969.05 (39.2)
	2015.05– 2016.03 (11)	1965.10– 1966.08 (11)	1983.08– 1984.05 (10)	1961.09– 1962.06 (10)	1999.11– 2000.08 (41.9)	1962.11– 1963.07 (38.7)	1994.02– 1994.07 (30.8)	1977.10– 1978.07 (36.8)
Asia	1975.05– 1977.12 (32)	2012.09– 2016.12 (52)	1977.09– 1984.04 (80)	1965.09– 1972.05 (81)	1975.05– 1977.12 (61.0)	2012.09– 2016.12 (65.4)	1977.09– 1984.04 (48.0)	1987.09– 1991.05 (47.6)
	1971.07– 1973.07 (25)	2006.11– 2009.05 (31)	1983.09– 1987.09 (49)	1959.06– 1964.06 (61)	1981.08– 1982.09 (41.9)	2000.10– 2002.12 (55.7)	2001.08– 2005.05 (43.8)	1959.06– 1964.06 (45.6)
	1987.03– 1988.12 (22)	2000.10– 2002.12 (27)	1961.07– 1965.07 (49)	1972.02– 1976.07 (54)	2002.08– 2004.02 (40.9)	2006.11– 2009.05 (45.2)	2012.04– 2015.06 (37.8)	1965.09– 1972.05 (39.8)
	1978.05– 1980.01 (21)	1960.12– 1962.09 (22)	1958.10– 1962.09 (48)	1987.09– 1991.05 (45)	1996.12– 1998.05 (39.5)	1958.07– 1960.04 (45.0)	1961.07– 1965.07 (34.7)	1996.06– 1999.04 (39.6)
	1950.10– 1952.06 (21)	1958.07– 1960.04 (22)	2001.08– 2005.05 (46)	1950.01– 1953.06 (42)	1971.07– 1973.07 (38.0)	1960.12– 1962.09 (35.1)	1983.09– 1987.09 (34.6)	2006.07– 2009.07 (37.9)
Europe	1962.07– 1964.05 (23)	2011.11– 2013.07 (21)	1958.09– 1961.05 (33)	1999.10– 2002.04 (31)	1953.10– 1954.06 (76.9)	2011.11– 2013.07 (62.7)	1987.11– 1989.09 (67.7)	2012.05– 2013.06 (64.2)
	1956.02– 1957.01 (12)	2009.06– 2011.02 (21)	1975.09– 1977.09 (25)	1965.07– 1967.06 (24)	1962.07– 1964.05 (70.1)	1996.12– 1997.12 (60.6)	1975.09– 1977.09 (65.7)	1998.06– 1999.07 (60.3)
	1976.03– 1977.02 (12)	1989.08– 1990.12 (17)	2001.12– 2003.11 (24)	1957.07– 1959.03 (21)	1976.03– 1977.02 (68.4)	1998.03– 1999.03 (60.5)	2005.06– 2006.11 (63.2)	1952.08– 1954.03 (58.1)
	1951.08– 1952.07 (12)	2006.10– 2007.10 (13)	1955.06– 1957.04 (23)	1992.08– 1994.04 (21)	1995.12– 1996.07 (66.8)	2009.06– 2011.02 (58.1)	1971.07– 1972.10 (62.3)	1981.06– 1982.07 (54.9)
	1996.07– 1997.05 (11)	1998.03– 1999.03 (13)	1987.11– 1989.09 (23)	1982.09– 1984.05 (21)	1971.09– 1972.05 (66.7)	2015.12– 2016.10 (53.5)	2001.12– 2003.11 (61.3)	1955.01– 1955.08 (54.0)
North America	1952.07– 1955.05 (35)	1961.04– 1962.11 (20)	1951.06– 1959.06 (97)	1984.09– 1989.07 (59)	1955.06– 1958.04 (75.5)	1976.12– 1978.05 (51.2)	1951.06– 1959.06 (83.2)	1984.09– 1989.07 (60.9)
	1955.06– 1958.04 (35)	1976.12– 1978.05 (18)	1968.07– 1971.07 (37)	1981.10– 1984.07 (34)	1952.07– 1955.05 (63.3)	1992.08– 1993.12 (51.1)	1976.05– 1977.07 (39.9)	2008.07– 2010.09 (52.4)
	1960.09– 1962.08 (24)	2003.12– 2005.04 (17)	1961.07– 1963.07 (25)	2008.07– 2010.09 (27)	1999.05– 2000.08 (56.0)	1996.09– 1997.06 (44.5)	1999.05– 2000.06 (39.9)	1992.06– 1994.03 (51.9)
	2001.09– 2003.06 (22)	1992.08– 1993.12 (17)	1961.06– 1963.06 (25)	1961.06– 1963.07 (26)	1958.02– 1959.03 (55.7)	1973.06– 1974.06 (43.9)	2012.02– 2013.04 (37.8)	1981.10– 1984.07 (50.9)
	1967.03– 1968.11 (21)	1950.12– 1952.04 (17)	1965.07– 1967.06 (24)	1978.06– 1980.05 (24)	1980.10– 1982.04 (53.9)	1998.01– 1999.03 (41.8)	2005.11– 2007.07 (36.7)	1959.06– 1960.07 (41.1)

TABLE S1. Continued.

Region	Duration (months)				Spatial extent (fraction %)			
	SPI based		SMPct based		SPI based		SMPct based	
	Drought	Pluvial	Drought	Pluvial	Drought	Pluvial	Drought	Pluvial
Oceania	2004.07– 2005.07 (13)	1973.06– 1974.07 (14)	1961.02– 1962.01 (12)	1973.04– 1974.11 (20)	2004.07– 2005.07 (90.7)	1973.06– 1974.07 (93.0)	1965.01– 1965.07 (80.7)	1973.04– 1974.11 (92.4)
	1972.02– 1973.01 (12)	1998.07– 1999.06 (12)	1982.05– 1983.02 (10)	2010.01– 2011.06 (18)	2002.03– 2003.02 (90.6)	1975.09– 1976.05 (89.9)	1951.11– 1952.06 (76.6)	1975.04– 1976.05 (88.7)
	2002.03– 2003.02 (12)	1950.03– 1951.02 (12)	2002.04– 2003.01 (10)	1975.04– 1976.05 (14)	1972.02– 1973.01 (90.4)	2010.07– 2011.05 (85.4)	2002.04– 2003.01 (75.9)	2010.01– 2011.06 (87.8)
	1977.02– 1977.12 (11)	2010.07– 2011.05 (11)	1972.01– 1972.09 (9)	1950.02– 1951.02 (13)	1994.05– 1994.12 (90.0)	1955.04– 1955.11 (83.9)	1994.04– 1994.12 (75.9)	1998.07– 1999.06 (82.2)
	1982.06– 1983.03 (10)	1975.09– 1976.05 (9)	1967.04– 1967.12 (9)	1998.07– 1999.06 (12)	1951.11– 1952.06 (80.8)	1998.07– 1999.06 (81.9)	1961.02– 1962.01 (74.5)	1968.04– 1968.09 (80.5)
South America	1966.12– 1968.09 (22)	1973.04– 1975.11 (32)	1957.11– 1959.05 (19)	2008.12– 2010.05 (18)	1963.04– 1964.05 (68.8)	1984.02– 1985.05 (62.4)	1967.07– 1968.10 (63.5)	1956.09– 1957.05 (50.1)
	1961.12– 1963.04 (17)	1981.11– 1984.01 (27)	1982.06– 1983.11 (18)	1982.06– 1983.08 (15)	1966.12– 1968.09 (66.7)	2008.12– 2010.03 (59.5)	2015.05– 2016.06 (59.7)	2007.10– 2008.05 (49.6)
	1958.01– 1959.05 (17)	2008.12– 2010.03 (16)	1967.07– 1968.10 (16)	1973.04– 1974.06 (15)	1988.02– 1989.04 (66.5)	1956.05– 1957.02 (58.9)	1951.04– 1952.03 (54.0)	1975.04– 1976.04 (48.8)
	1982.08– 1983.12 (17)	1984.02– 1985.05 (16)	2015.05– 2016.06 (14)	1989.05– 1990.05 (13)	2015.07– 2016.08 (66.4)	1981.11– 1984.01 (58.8)	1988.01– 1988.09 (53.5)	1973.04– 1974.06 (47.7)
	1988.02– 1989.04 (15)	2015.05– 2016.06 (14)	1951.04– 1952.03 (12)	1975.04– 1976.04 (13)	1951.01– 1952.03 (54.2)	1973.04– 1975.11 (55.9)	1963.03– 1963.12 (53.0)	2008.12– 2010.05 (47.6)

References

- Alfieri, L., E. Zsoter, S. Harrigan, F. A. Hirpa, C. Lavaysse, C. Prudhomme, and P. Salamon, 2019: Range-dependent thresholds for global flood early warning. *J. Hydrol. X*, **4**, 100034, <https://doi.org/10.1016/J.HYDROA.2019.100034>.
- Brakenridge, G. R., 2019: Global active archive of large flood events, Dartmouth Flood Observatory, accessed 6 January 2019, www.dartmouth.edu/~floods/Archives/index.html.
- Do, H. X., L. Gudmundsson, M. Leonard, S. Westra, and W. Grabs, 2018: The Global Streamflow Indices and Metadata Archive (GSIM)—Part 1: The production of a daily streamflow archive and metadata. *Earth Syst. Sci. Data*, **10**, 765–785, <https://doi.org/10.5194/essd-10-765-2018>.
- Gudmundsson, L., H. X. Do, M. Leonard, and S. Westra, 2018: The Global Streamflow Indices and Metadata Archive (GSIM)—Part 2: Quality control, time-series indices and homogeneity assessment. *Earth Syst. Sci. Data*, **10**, 787–804, <https://doi.org/10.5194/essd-10-787-2018>.
- Pappenberger, F., E. Dutra, F. Wetterhall, and H. L. Cloke, 2012: Deriving global flood hazard maps of fluvial floods through a physical model cascade. *Hydrol. Earth Syst. Sci.*, **16**, 4143–4156, <https://doi.org/10.5194/hess-16-4143-2012>.
- Winsemius, H., L. Van Beek, B. Jongman, P. Ward, and A. Bouwman, 2013: A framework for global river flood risk assessments. *Hydrol. Earth Syst. Sci.*, **17**, 1871–1892, <https://doi.org/10.5194/hess-17-1871-2013>.